Tunable band topology in gyroscopic lattices

Noah P. Mitchell,[1,*] Lisa M. Nash,[1] and William T. M. Irvine[1,2,†]
[1]*James Franck Institute and Department of Physics, University of Chicago, Chicago, Illinois 60637, USA*
[2]*Enrico Fermi Institute, The University of Chicago, Chicago, Illinois 60637, USA*

(Received 29 July 2018; published 5 November 2018)

Gyroscopic metamaterials, mechanical structures composed of interacting spinning tops, have recently been found to support one-way topological edge waves. In these structures, the time-reversal symmetry breaking that enables their topological behavior emerges directly from the lattice geometry. Here we show that variations in the lattice geometry can give rise to more complex band topology than has been previously described. A "spindle" lattice (or truncated hexagonal tiling) of gyroscopes possesses both clockwise and counterclockwise edge modes distributed across several band gaps. Tuning the interaction strength or twisting the lattice structure along a Guest mode opens and closes these gaps and yields bands with Chern numbers of $|C| > 1$ without introducing next-nearest-neighbor interactions or staggered potentials. A deformable honeycomb structure provides a simple model for understanding the role of lattice geometry in constraining the effects of time-reversal symmetry and inversion symmetry breaking. Last, we find that topological band structure generically arises in gyroscopic networks, and a simple protocol generates lattices with topological excitations.

DOI: 10.1103/PhysRevB.98.174301

I. INTRODUCTION

Materials with nontrivial band topology have captured the attention of condensed-matter scientists since their discovery in electronic systems [1]. Since then, the concept of topological order has found its way to a plethora of physical systems, from electronic to photonic, acoustic, and even mechanical systems [2–14]. When topologically nontrivial, all these systems exhibit excitations confined to their surface that propagate unidirectionally without backscattering and are robust to disorder. These features both are fundamentally intriguing and form the basis for technological applications of topological materials.

Here we focus on unidirectional edge modes in structures composed of coupled spinning objects [4–6,15–17]. In particular, we focus on the topological properties arising from the collective motion of lattices of gyroscopes – namely, how their phononic band structure encodes a nonzero Chern number. When the band structure is topologically nontrivial, the gyroscopic system supports unidirectional waves on its boundary. These edge waves are distinct from a range of other nonreciprocal properties that emerge in angular-momentum-biased systems because of their topological origin [18,19].

The minimal requirements for such a Chern insulator are the presence of a band gap and broken time-reversal symmetry. In the electronic case, time-reversal symmetry breaking arises from the presence of magnetic fields [20]. As we will see, the analogous mechanism in gyroscopic lattices is the lattice geometry itself: the mere presence of spinning components is not sufficient to generate the effects enabling chiral edge modes.

In this paper, we go beyond simple geometries and find the flexibility to design lattices with desired band gaps and desired topology. In particular, we examine tunable lattices with Chern numbers $|C| > 1$ as well as multiple gaps with edge modes of opposite chirality. We examine the effects of competing time-reversal symmetry breaking with inversion symmetry breaking and demonstrate a design strategy to achieve band topology in lattices with seemingly arbitrary unit cells.

II. THE EQUATIONS OF MOTION

A simple realization of gyroscopic metamaterials is a collection of coupled gyroscopes which hang from a pivot point and spin rapidly enough for their angular momentum to lie approximately along the primary axis, as shown in Fig. 1(a). Under these conditions, the free tip of a gyroscope moves when a torque $\vec{\tau}$ acts about the pivot point according to

$$\vec{\tau} \approx I\omega\dot{\hat{n}} = \vec{\ell}_f \times \vec{F}, \tag{1}$$

where I is the principal moment of inertia, ω is the spinning speed, $\hat{n}$ is a unit vector pointing from the pivot point toward the center of mass, and $\vec{\ell}_f$ is the vector from the pivot point to the point acted upon by force $\vec{F}$.

Considering small displacements of each gyroscope allows a linearized description. Denoting the displacement from the equilibrium position in the plane as $\psi = x + iy$, the equation of motion for a single gyroscope under the influence of gravity becomes

$$i\dot{\psi} = \frac{mg\ell_{cm}}{I\omega}\psi. \tag{2}$$

Note that throughout this paper, without loss of generality, we choose the angular momentum vector of a hanging gyroscope to point down, from the pivot point towards the center of mass.

*Corresponding author: npmitchell@uchicago.edu
†Corresponding author: wtmirvine@uchicago.edu

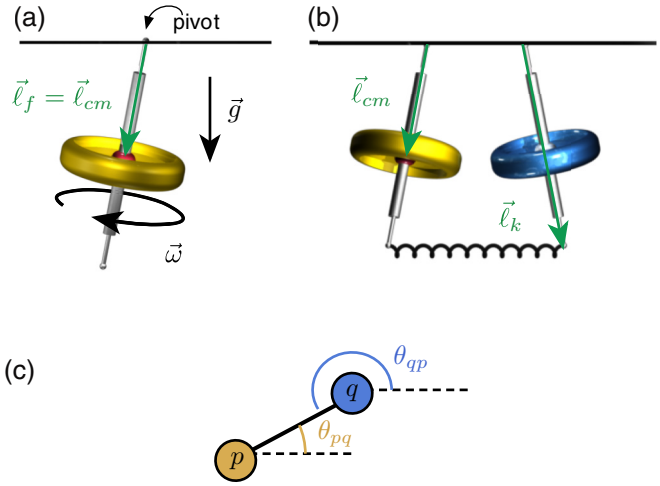

FIG. 1. A spring-coupled gyroscopic metamaterial is composed of spinning gyroscopes that hang from a pinned pivot point. (a) $\vec{\ell}_f$ is the vector from the pivot point to where a force acts. When the only force is gravity, $\vec{\ell}_f = \vec{\ell}_{cm}$. (b) Gyroscopes in the metamaterial are coupled to their neighbors in the lattice via a spring which is attached to the free end. (c) The linearized equation of motion for our system relates the displacements via angles between bonds and the local gyroscope's local x axis (indicated by dotted lines in this view from below).

Noting the similarity between Eq. (2) and the Schrödinger equation for a quantum particle, we use the same notion of time-reversal symmetry as is used in quantum mechanics, namely, $\psi \to \psi^*$ and $t \to -t$. While $\psi \to \psi^*$ corresponds to a reversal of momentum for a quantum particle, in the context of gyroscopes, $\psi \to \psi^*$ carries out a reflection of the gyroscope's displacement about a horizontal axis passing through its pivot point. Performing this operation on the equation above, we find that Eq. (2) is time reversal symmetric. Thus, a spinning top precessing under the influence of gravity does not break this notion of time-reversal symmetry.

Introducing interactions, however, allows the structure to break time-reversal symmetry. The simplest setting to see this is a network of gyroscopes coupled by linear springs. For small displacements, the forces exerted on one gyroscope by another are proportional to the component of the net displacement along the line connecting them. For a given pair of gyroscopes p and q, it is convenient to extract the component of the net displacement $\psi_p - \psi_q$ along the bond by rotating the system to the local x-axis of p, taking the real part of the expression, and then rotating back. The resulting force in complex form is given by

$$\begin{aligned} F_{pq} &= -k_0 e^{i\theta_{pq}} \mathrm{Re}[e^{-i\theta_{pq}}(\psi_p - \psi_q)] \\ &= -\frac{k_0 e^{i\theta_{pq}}}{2}[e^{-i\theta_{pq}}(\psi_p - \psi_q) + e^{i\theta_{pq}}(\psi_p^* - \psi_q^*)], \end{aligned} \quad (3)$$

where k_0 is the spring constant of the bond. Using this result, the equation of motion for two gyroscopes can then be written as

$$i\dot{\psi}_p = \Omega_g \psi_p + \frac{\Omega_k}{2}[(\psi_p - \psi_q) + e^{2i\theta_{pq}}(\psi_p^* - \psi_q^*)], \quad (4)$$

where $\Omega_k = k_0 \ell_k^2/(I\omega)$ and $\Omega_g = mg\ell_{cm}/(I\omega)$. We define the time-reversal operation as $\psi_p^{TR}(t) = \psi_p^*(-t)$. By taking the complex conjugate of $\dot{\psi}_p$ and rewriting in terms of ψ_p^{TR}, we see that the equations of motion are changed only by $e^{i2\theta} \to e^{-i2\theta}$. Therefore, we see that time-reversal symmetry is preserved under reflections that are parallel or perpendicular to the bond [4].

The full equation of motion for a hanging gyroscope with more than one neighbor can be similarly expressed:

$$i\dot{\psi}_p = \Omega_g \psi_p + \frac{\Omega_k}{2}\sum_q^{n.n.}[(\psi_p - \psi_q) + e^{2i\theta_{pq}}(\psi_p^* - \psi_q^*)]. \quad (5)$$

As before, time-reversal symmetry is preserved only if all bonds are either parallel or perpendicular to each other since, in this case, a coordinate system can be chosen so that bonds lie along the x and y axes, constraining the prefactor $e^{2i\theta_{pq}}$ to be real for all bonds in the network.

To date, the only ordered lattices that have been considered in this framework are the honeycomb lattice and simple distortions thereof [4,5]. A slightly different manifestation of gyroscopic metamaterials considered in Ref. [6] found that by including staggered sublattice precession frequencies and bond strengths, time-reversal symmetry could be effectively broken in lattices with square and honeycomb symmetries.

III. TWISTED SPINDLE LATTICE

To demonstrate the considerable flexibility of gyroscopic metamaterials, we begin by considering the twisted spindle lattice shown in Fig. 2. This structure shares features of both the honeycomb lattice and the kagome lattice. As Fig. 2(a) shows, shrinking the blue triangles to a single site while increasing the strength of blue bonds deforms the spindle lattice into the honeycomb lattice. Conversely, taking the length of the red bonds that connect triads of gyroscopes to zero while increasing their strength deforms the spindle lattice into a kagome configuration. As shown in Fig. 2(b), the spindle lattice also supports a Guest mode – a global elastic distortion that costs no energy – in which each triad of gyroscopes rotates locally.

In the limiting case of the honeycomb lattice, which has two sites per unit cell, we find a single gap with clockwise topologically protected edge modes [4]. By contrast, in the kagome lattice, with three sites per unit cell, there are two gaps, which each support a counterclockwise topological mode, as shown in the Supplemental Material [21]. In the intermediate case of the undeformed spindle lattice, which has six sites per unit cell, we generically find five band gaps. Most of these gaps possess chiral edge modes, and a given configuration can host both clockwise and counterclockwise modes. As we show below, locally twisting this structure [as in Fig. 2(b)] or varying the bond strengths Ω_k relative to the pinning strength Ω_g opens and closes edge-mode-carrying gaps.

Shaking a gyroscope on the boundary of this network at a frequency in the lowest band gap generates a clockwise wave packet confined to the edge of the sample which is robust to disorder in the gravitational precession frequencies or bond strengths and does not scatter at sharp corners or defects (Fig. 3(a) and Video 1 in the Supplemental Material [21]).

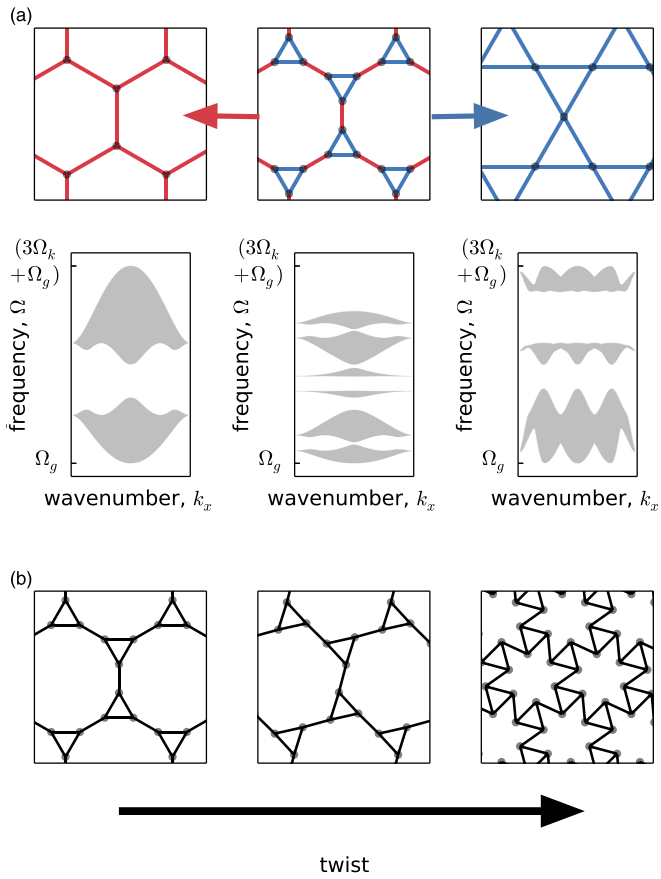

FIG. 2. The spindle lattice shares features of both the honeycomb and kagome lattices while supporting a Guest mode in which each triad of gyroscopes is locally rotated. (a) Taking the size of the red triangles in the spindle lattice to zero returns a honeycomb configuration, while taking the length of the blue bonds connecting each red triangle of gyroscopes to zero transforms the spindle lattice into the kagome configuration. The associated band structures are shown below each of the three configurations. (b) Locally twisting the triangles of a spindle lattice preserves bond lengths while globally deforming the lattice.

Shaking at a frequency in the middle band gap, however, generates counterclockwise edge waves, allowing a single lattice structure to conduct protected edge waves with a chirality determined by frequency [Fig. 3(b)]. We compute the Chern number for each band via [22]

$$C_j dx \wedge dy = \frac{i}{2\pi} \int d^2k \, \mathrm{Tr}[dP_j \wedge P_j dP_j], \qquad (6)$$

where P_j is the projection matrix defined using a symplectic inner product between states (see the Supplemental Material [21]) and $\wedge$ is the wedge product. We note that the use of symplectic norms for the projector in our system was absent in previous studies of gyroscopic lattices. We find that the Chern number is equal to the number of chiral edge modes, which suggests the same bulk-boundary correspondence for these systems as in electronic Chern insulators [15,23].

The topological band structure of the gyroscopic spindle lattice offers additional axes of tunability through varying the interaction strength (i.e., the bond stiffness in the case of springs) and by performing bond-length-preserving deformations on the lattice. For gyroscopic lattices with uniform interaction strengths (i.e., equal spring constants throughout), we can tune the ratio of the interaction frequency to gravitational precession frequency Ω_k/Ω_g. This operation can close band gaps in addition to changing the frequency range of the band structure. In the case of the spindle lattice, this provides a tuning knob that changes the topology of the band structure. Simply increasing the interaction strength relative to the gravitational precession frequency closes and reopens gaps and changes the Chern numbers of bands, as shown in Fig. 4(a). We note that this feature was absent in the gyroscopic honeycomb lattice previously studied [4,5], whose topology was unaffected by changes in Ω_k and Ω_g. This allowed the topology to be continuously connected to the electronic Haldane model, unlike in the spindle lattice.

Twisting the spindle lattice through a Guest mode, as shown in Fig. 2(b), also provides a tuning knob. Globally deforming the lattice closes and reopens the lowest and highest band gaps, allowing for several distinct configurations of multiple gaps supporting protected chiral edge modes, as shown in Fig. 4(c) and Video 2 in the Supplemental Material [21]. As the twist angle grows, there are five values for which a pair of bands touch and reopen, flipping the chirality of the modes in that gap or imparting chiral modes to a gap which previously had none.

What determines the chirality of edge modes? Unlike in the topological zero-energy modes recently found in Maxwell lattices [8], here the coordination number alone does not play a central role in determining band topology. If Chern numbers were determined purely by the number of nearest neighbors, we would expect, for instance, that the spindle and honeycomb lattices would have similar edge modes: both have a coordination number of $z = 3$. However, the spindle supports edge modes of either chirality. Furthermore, the spindle lattice's rich band structure depends not only on geometry but also bond strengths [Fig. 3(a)]. We conclude that simple, local aspects of the lattice such as coordination number and mean bond angle do not singlehandedly determine the band structure.

From a design perspective, the two simple tuning parameters of angle and interaction strength are sufficient to cover a broad range of topological phenomenology without introducing staggered interaction strengths, including edge modes with either chirality, the opening and closing of gaps, and bands with Chern numbers of ± 1 and ± 2. These behaviors demonstrate the versatility of gyroscopic metamaterials.

IV. TIME-REVERSAL SYMMETRY AND TOPOLOGICAL BAND GAPS

All configurations shown so far break time-reversal symmetry, which is a necessary ingredient for band topology in Chern insulators [4,6]. This is not necessarily true for all gyroscopic lattices. For example, as illustrated in Fig. 5, a honeycomb lattice can undergo a bond-length-preserving deformation to a configuration in which all bond angles are multiples of $\pi/2$ (for $\delta = \pi$). In such a configuration, time-reversal symmetry is restored, and therefore, band topology

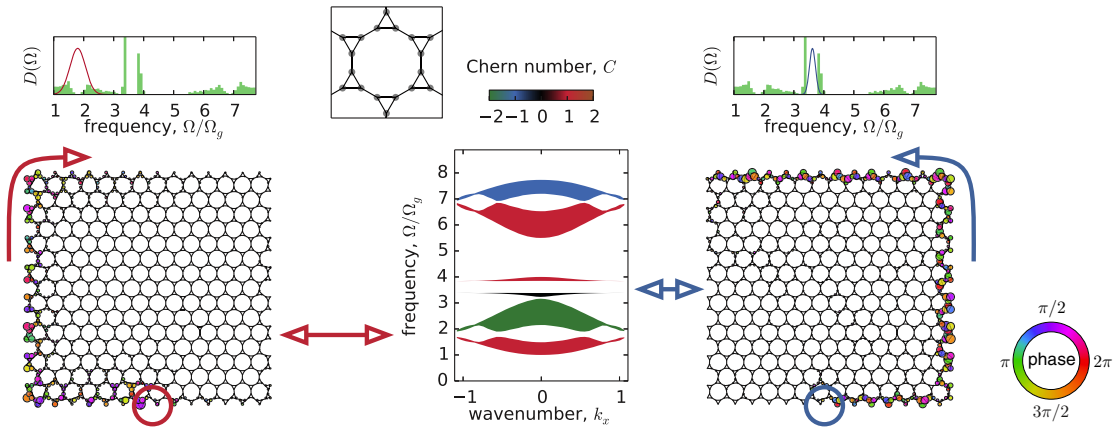

FIG. 3. The gyroscopic spindle lattice contains chiral edge modes of either chirality as well as band with a Chern number of $|C| > 1$. Direct simulation of Eq. (5) reveals clockwise (left) and counterclockwise (right) edge modes in the same structure when shaken at different frequencies [$\Omega = 1.8\,\Omega_g$ (left) and $3.62\,\Omega_g$ (right)]. The displacement of each gyroscope is represented as a circle with a radius proportional to the displacement's magnitude. The color of each circle represents the phase of the displacement, as depicted in the color wheel on the bottom right. Computing the Chern numbers for each band confirms the topological origin of the chiral edge modes, as shown by the colored band structure in the middle panel. A single gyroscope on the edge is shaken at a fixed frequency with an amplitude varying in time; the spectrum of the excitation is indicated by red (left) and blue (right) curves overlying the density of states $D(\Omega)$. The density of states, shown above each lattice, is given for the case with periodic boundary conditions. For these simulations, the interaction strength was set to $\Omega_k = 3\Omega_g$.

disappears. Further changing the value of δ past π causes the band topology to reappear, but with opposite sign. In Fig. 5, we extend this analysis to the entire phase space of periodic, bond-length-preserving deformations by introducing

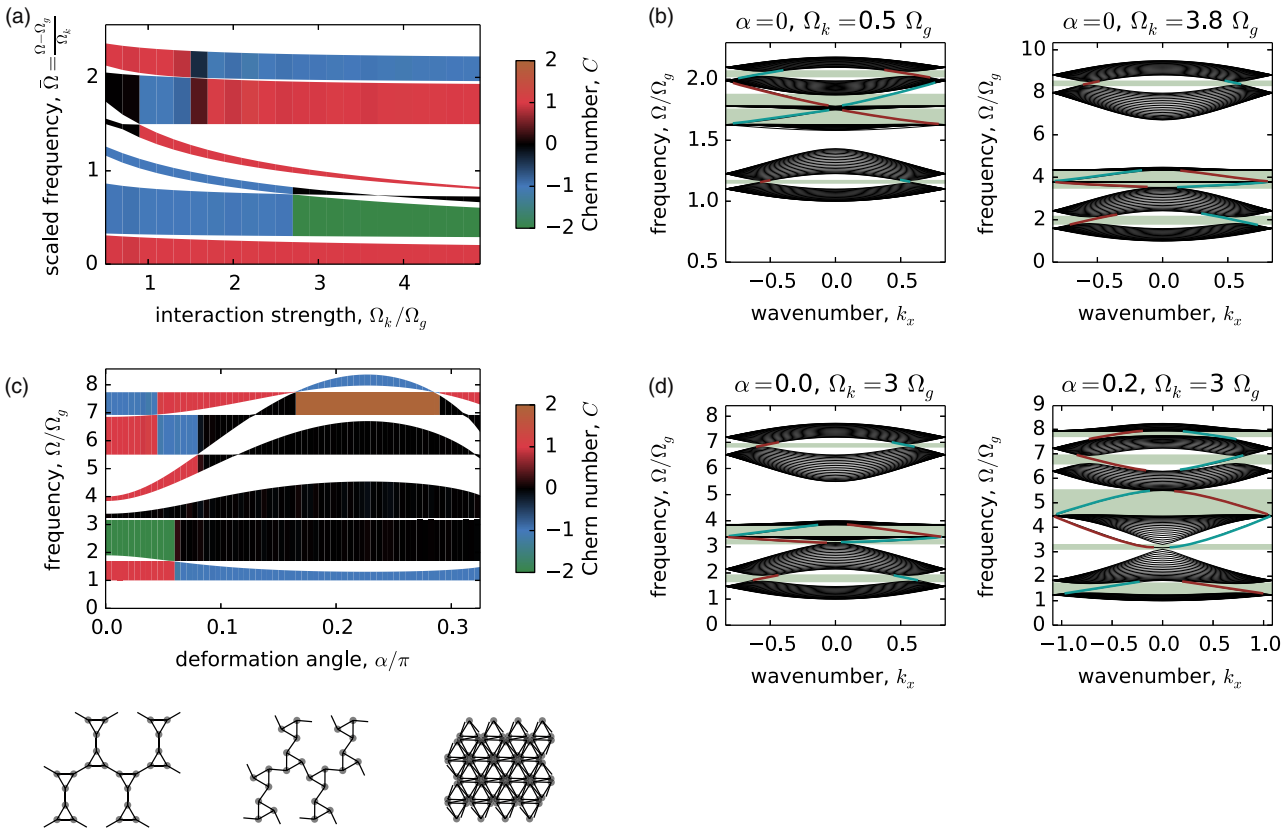

FIG. 4. Phononic band structures for the spindle and twisted spindle lattices show the opening and closing of gaps with topological edge states. (a) Simply increasing the interaction strength enables the closing and opening of band gaps, creating and annihilating protected chiral edge modes. (b) Band gaps with chiral edge modes are highlighted in green for two different interaction strengths. (c) and (d) As the structure is twisted through a bond-length-preserving deformation, three of the five gaps close and reopen, leading to three or four gaps with chiral edge modes, depending on the value of the twist deformation angle α. In (c) and (d), we set $\Omega_k = 3\Omega_g$.

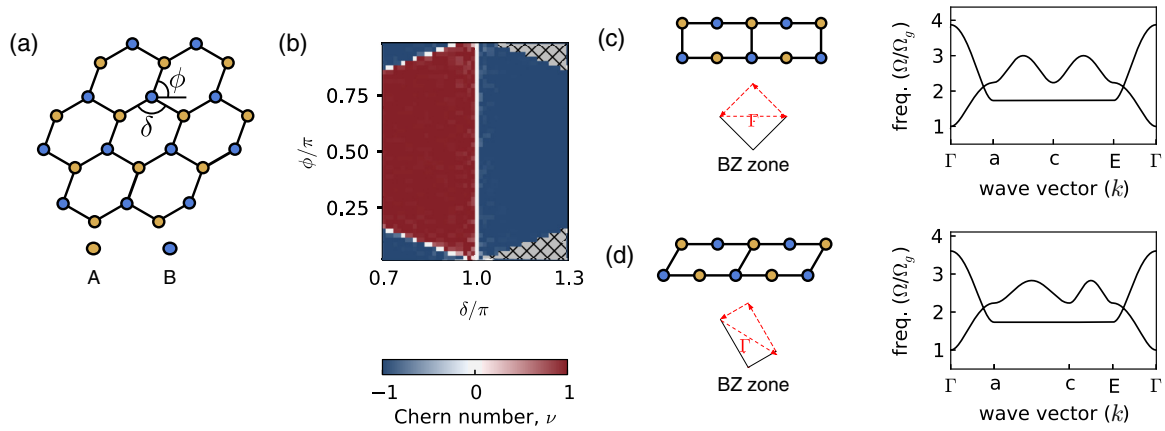

FIG. 5. Band gaps and topology in the deformed honeycomb lattice. (a) The angles ϕ and δ control the deformation of the honeycomb lattice. (b) The ϕ-δ phase diagram shows that the Chern number of the lower band changes when straight lines of bonds appear in the lattice, which occurs on the white diagonal lines in the left corners and on the white vertical line at $\delta = \pi$. (c) The bricklayer configuration ($\delta = \pi$) band structure is plotted along paths in the Brillouin zone. The gap is closed at two Dirac points. (d) No band gap opens in the canted brick layer ($\delta = \pi$, $\phi \neq \pi/2$), even though time-reversal symmetry is broken in this configuration.

an additional angle, ϕ. This allows us to explore the question of whether time-reversal symmetry breaking is sufficient to generate band topology in gyroscopic metamaterials.

Figure 5(b) shows the topological phase diagram corresponding to general deformations of the honeycomb lattice, characterized by angles ϕ and δ. Red (blue) regions indicate a Chern number of 1 (-1) for the lower band and, correspondingly, clockwise (counterclockwise) propagating modes in the gap. For $\phi = \pi/2$ and $\delta = \pi$, the network is arranged in a brick-layer configuration [Fig. 5(c)]. Varying either ϕ or δ from this point breaks time-reversal symmetry. However, only changes in δ imbue nontrivial band topology, as illustrated by the white line in Fig. 5(b) for $\delta = \pi$ [4]. The fact that changes in ϕ break time-reversal symmetry without opening a gap demonstrates that broken time-reversal symmetry does not inevitably lead to either band gaps or nontrivial band topology.

This behavior warrants further investigation. During the deformation of the honeycomb into the brick-layer geometry, the band gap closes, and the two Dirac points in the spectrum touch at a point. Surprisingly, these Dirac points are preserved even in the canted brick-layer configuration, as shown in Fig. 5(d), despite the fact that shearing the brick-layer configuration breaks time-reversal symmetry by creating acute and obtuse bond angles [see Eq. (5)].

As detailed in the Supplemental Material, this protection of the Dirac cones arises due to a subtle pseudoreflection symmetry. The symmetry consists of reflecting the positions of gyroscopes about the x axis and shearing their relative positions such that the tilt angle ϕ is invariant, while leaving the gyroscopes' displacements unchanged. This pseudoreflection is a symmetry of the equations of motion and thus of the normal modes [21]. This symmetry leads to the existence of a special line of modes in momentum space. Along this line, modes that are symmetric and antisymmetric under the symmetry operation decouple and cannot hybridize at their band crossing. Thus, a pseudoreflection symmetry stabilizes the Dirac points against acquiring gaps, which would otherwise be unstable to time-reversal symmetry-breaking perturbations, analogous to the effect of other discrete symmetries in electronic systems [24]. The pseudoreflection symmetry also explains the vanishing Chern number for all values of ϕ at $\delta = \pi$ seen in Fig. 5(b) because the Berry curvature is odd under the action of the symmetry. More broadly, this protection underscores the interplay between lattice geometry and the topological character of the band structure.

V. COMPETING SYMMETRIES IN TOPOLOGICAL GYROSCOPIC SYSTEMS

Breaking inversion symmetry is the canonical mechanism for opening gaps in the phonon spectra of mass-and-spring lattices [25]. This is also true in other systems, such as electronic materials. This gap-opening mechanism can be made to compete with broken time-reversal symmetry to close and reopen gaps and eliminate protected chiral edge modes. To study an analogous effect in gyroscopic lattices, we detune the yellow and blue sublattice sites in Fig. 6 by modulating their on-site gravitational precession frequencies: $\Omega_{gA,B} = (1 \pm \Delta)\Omega_g$ (see also [5]).

Figure 6(a) shows the phase diagram that results from varying δ and lattice pinning frequencies $\Omega_{gA,B}$. When the unit cell's two sites are equivalent ($\Delta = 0$), the Chern number of the system changes only when the gap closes at the brick-layer transition. For $\Delta \neq 0$, however, a third, topologically trivial region appears. In this case, the band structure is gapped but displays no chiral edge modes.

The behavior of excitations confirms the Chern number calculations in all three regions, as indicated in Figs. 6(b)–6(d) and Video 3 in the Supplemental Material [21]. In Fig. 6(c), excitations propagate along the edge in both directions. The Chern number is zero, and these edge waves are not topologically protected: they backscatter at sharp corners or in the presence of disorder (see Video 4 in the Supplemental Material [21]). The result shown in Fig. 6(a) displays a strong resemblance to Haldane's phase diagram: sites must have similar pinning strengths for the lattice to support topological states.

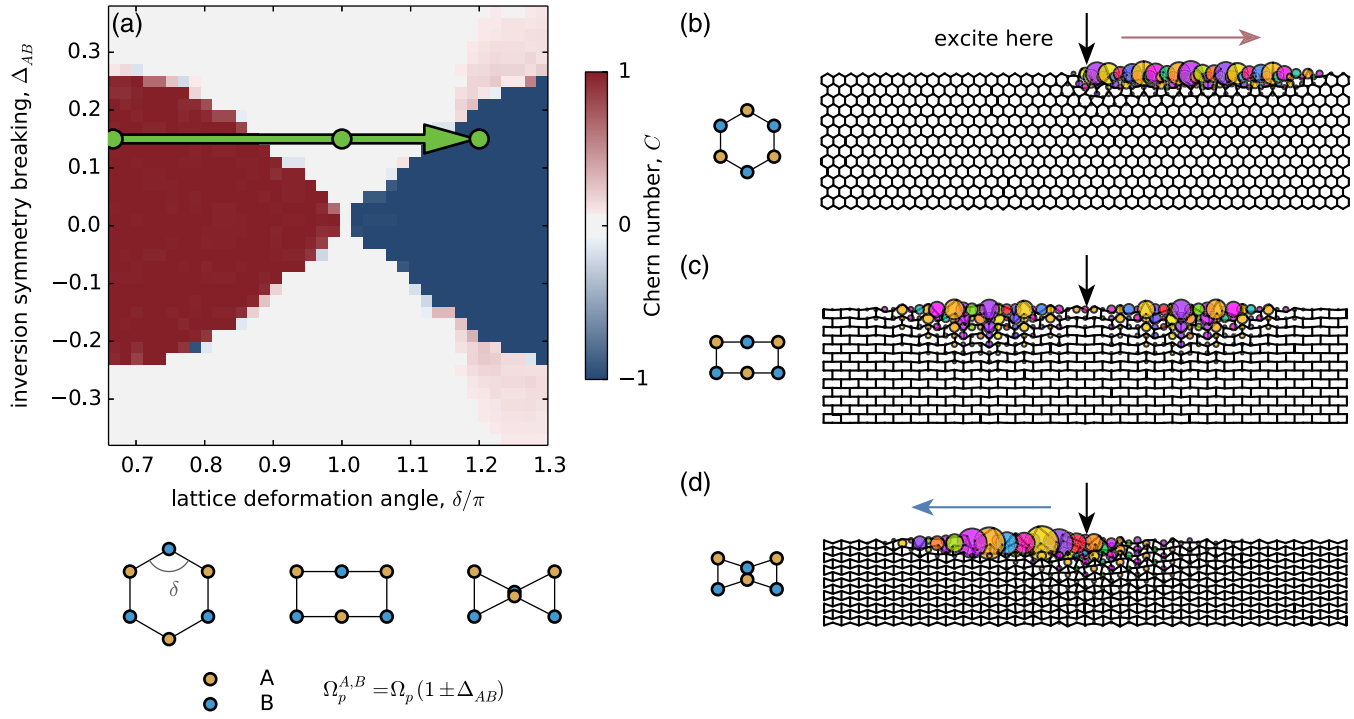

FIG. 6. Inversion and time-reversal symmetries compete in a gyroscopic lattice. (a) The phase diagram for a deformed honeycomb lattice (without shear, so that $\phi = \pi/2$) with varying Ω_g values on sites A and B shows an interplay between inversion and time-reversal symmetries. (b) In a simulation of the honeycomb lattice with inversion symmetry breaking $\Delta_{AB} = 0.15$, driving a gyroscope on the edge at a gap frequency results in a clockwise wave packet. (c) When the lattice is deformed to a brick-layer geometry, the Chern number vanishes. This configuration is gapped due to the inversion symmetry breaking ($\Delta_{AB} = 0.15$). The gap contains modes which are localized on the edge, but these unprotected edge waves propagate in both directions and are not robust against disorder. (See also Videos 3 and 4 in the Supplemental Material.) (d) In the bow-tie geometry, edge modes propagate counterclockwise, as predicted by the calculations shown in (a).

While varying precession frequencies is an effective way of breaking inversion symmetry, it is not the only one. An alternative way is to alter the coordination number between sites, i.e., the number of bonds that are linked to each gyroscope. For example, unlike the lattices considered so far, the α-$(ET)_2I_3$ lattice shown in Fig. 7 contains sites of coordination number $z = 4$ (for sites A and B) and $z = 2$ (for sites C and D). When all gravitational precession frequencies are equal, the lattice displays no topological excitations [top right corner of Fig. 7(b)].

As seen in the first term of Eq. (5), contributions to on-site pinning, i.e. terms in which $\dot{\psi}_p$ depends on ψ_p, come not only from gravitation precession terms Ω_g but also from coupling to adjacent sites. For lattices with unequal coordination at different sites, balancing the full "site pinning frequency" Ω_p for each site can be used to enhance or remedy the effects of site inequivalence:

$$\Omega_p \equiv z\frac{\Omega_k}{2} + \Omega_g. \tag{7}$$

We can test if site pinning inequivalence is the mechanism preventing the α-$(ET)_2I_3$ lattice from having gaps. Indeed, reducing the precession frequencies of the sites with higher coordination numbers enables a band gap with chiral edge modes [Fig. 7(b)]. This provides another example of the inextricable connection between lattice geometry and topological order in gyroscopic lattices.

VI. TOWARDS TOPOLOGICAL DESIGN

We have seen that both time-reversal symmetry and site equivalence are tied to lattice geometry and connectivity. Turning now to engineering new topological gyroscopic lattices, we can summarize the principles of the previous sections as follows:

(i) Breaking time-reversal symmetry via bond angles is a necessary, but not sufficient, condition for creating a lattice with a nontrivial band topology.

(ii) A competition between time-reversal symmetry and site equivalence determines whether or not a lattice can have topological modes. Lattice connectivity is relevant for determining the effective on-site precession frequencies to achieve equivalence.

Using these two principles, one can construct topological metamaterials beginning with an arbitrary unit cell and subsequently balancing pinning frequencies according to Eq. (7). This procedure can generate lattices with desired properties, such as multiple band gaps or mechanical stability. Figure 8 shows several examples, including a deformed kagome lattice, which has gained considerable interest for its versatile mechanical properties [8,26–28].

One example of a mechanically stable lattice with nonvanishing Chern number is shown in Fig. 8(b). Although all previous lattices in this paper have been mechanically unstable ($\bar{z} \leqslant 4$), the lattice in Fig. 8(b) shows that this is not necessary for band topology to arise. Sublattices A

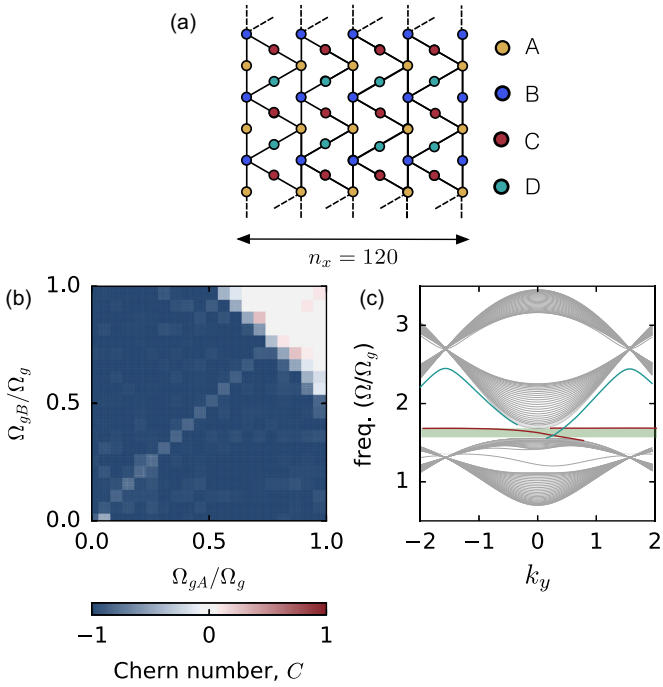

FIG. 7. Coordination number and topological phases. (a) A lattice with four lattice sites per unit cell, where sites A and B have two neighbors and sites C and D have two. (b) The topological phase diagram for varying the gravitational precession frequencies on sites A and B shows that because of the different coordination numbers for the lattice sites, the band structure is trivial when $\Omega_{gA} = \Omega_{gB} = \Omega_{gC} = \Omega_{gD}$. (c) The band structure in the nontrivial phase for a strip which is infinite along y and 120 unit cells wide in x.

(yellow) and C (red) have five bonds each, while sublattice B (blue) has four. We expect that topological modes will arise when the total pinnings for all sites are approximately equal, which would occur for $\Omega_B > \Omega_{A,C}$. Figure S6 in the Supplemental Material shows that the numerics agree with this prediction [21].

The results demonstrated in this section show that topology is not specific to one family of lattices in gyroscopic networks and is, in fact, ubiquitous. Many topological lattices can be created using only simple principles, opening myriad possibilities for material design.

VII. CONCLUSION

In this paper, we explored the interplay between lattice geometry and topological order in gyroscopic lattices, including the effects of broken time-reversal symmetry and site equivalence. Along the way, we found examples of lattices with multiple band gaps containing edge modes of either chirality in the same structure and Chern numbers $|C| > 1$. We then identified general principles which are helpful in designing lattices with desired topological band structures. Building on our observations, we used a simple prescription that yields mechanically stable topological gyroscopic lattices and lattices with multiple band gaps. The ubiquity of band topology in gyroscopic metamaterials provides a broad palette with which to design topological behaviors in elastic structures. Further study could investigate the interplay between band topology and nonlinear excitations in gyroscopic networks or interspersing both clockwise and counterclockwise spinning sites.

ACKNOWLEDGMENTS

We thank A. Turner for providing the argument of Dirac cone protection in the canted brick-layer lattice, for point-

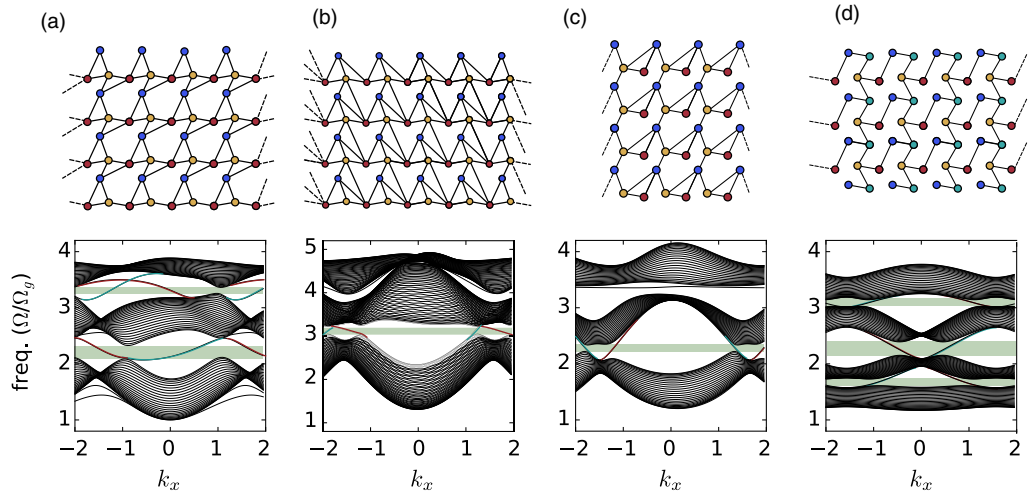

FIG. 8. Examples of topological lattices created balancing coordination by varying on-site precession frequencies. Each lattice is generated by placing triangulated points in a square unit cell, then deleting some bonds randomly. (a) An example of a deformed kagome lattice structure exhibits two topological gaps. (b) A mechanically stable lattice with one topological gap (upper gap) demonstrates that gyroscopic lattices need not be undercoordinated to be Chern insulators. The propagation of edge modes is in the same direction as the kagome lattice. (c) A three-site-per-unit-cell lattice structure with one topological gap (lower gap). The propagation of edge modes is in the same direction as the honeycomb lattice. (d) An example of a four-site-per-unit-cell lattice structure with three topological gaps. The propagation of edge modes is in the same direction as the kagome lattice for all three gaps.

ing out the symplectic symmetry of our system and its interpretation, for detailed comments on the manuscript, and for useful discussions. We also thank A. Souslov for useful discussions. This work was primarily supported by the University of Chicago Materials Research Science and Engineering Center, which is funded by the National Science Foundation under Award No. DMR-1420709. Additional support was provided by the Packard Foundation. This work was also supported by NSF EFRI NewLAW Grant No. 1741685.

[1] D. J. Thouless, M. Kohmoto, M. P. Nightingale, and M. den Nijs, Phys. Rev. Lett. **49**, 405 (1982).
[2] E. Prodan and C. Prodan, Phys. Rev. Lett. **103**, 248101 (2009).
[3] M. C. Rechtsman, J. M. Zeuner, Y. Plotnik, Y. Lumer, D. Podolsky, F. Dreisow, S. Nolte, M. Segev, and A. Szameit, Nature (London) **496**, 196 (2013).
[4] L. M. Nash, D. Kleckner, A. Read, V. Vitelli, A. M. Turner, and W. T. M. Irvine, Proc. Natl. Acad. Sci. USA **112**, 14495 (2015).
[5] N. P. Mitchell, L. M. Nash, and W. T. M. Irvine, Phys. Rev. B **97**, 100302 (2018).
[6] P. Wang, L. Lu, and K. Bertoldi, Phys. Rev. Lett. **115**, 104302 (2015).
[7] S. H. Mousavi, A. B. Khanikaev, and Z. Wang, Nat. Commun. **6**, 8682 (2015).
[8] C. L. Kane and T. C. Lubensky, Nat. Phys. **10**, 39 (2013).
[9] R. Süsstrunk and S. D. Huber, Science **349**, 47 (2015).
[10] F. D. M. Haldane and S. Raghu, Phys. Rev. Lett. **100**, 013904 (2008).
[11] J. Ningyuan, C. Owens, A. Sommer, D. Schuster, and J. Simon, Phys. Rev. X **5**, 021031 (2015).
[12] V. Peano, C. Brendel, M. Schmidt, and F. Marquardt, Phys. Rev. X **5**, 031011 (2015).
[13] Z. Wang, Y. D. Chong, J. D. Joannopoulos, and M. Soljačić, Phys. Rev. Lett. **100**, 013905 (2008).
[14] R. Fleury, A. B. Khanikaev, and A. Alú, Nat. Commun. **7**, 11744 (2016).
[15] N. P. Mitchell, L. M. Nash, D. Hexner, A. M. Turner, and W. T. M. Irvine, Nat. Phys. **14**, 380 (2018).
[16] A. B. Khanikaev, R. Fleury, S. H. Mousavi, and A. Alú, Nat. Commun. **6**, 8260 (2015).
[17] A. Souslov, B. C. V. Zuiden, D. Bartolo, and V. Vitelli, Nat. Phys. **13**, 1091 (2017).
[18] R. Fleury, D. L. Sounas, C. F. Sieck, M. R. Haberman, and A. Alú, Science **343**, 516 (2014).
[19] S. Maayani, R. Dahan, Y. Kligerman, E. Moses, A. U. Hassan, H. Jing, F. Nori, D. N. Christodoulides, and T. Carmon, Nature (London) **558**, 569 (2018).
[20] F. D. M. Haldane, Phys. Rev. Lett. **61**, 2015 (1988).
[21] See Supplemental Material at http://link.aps.org/supplemental/10.1103/PhysRevB.98.174301 for additional information and videos.
[22] J. E. Avron, R. Seiler, and B. Simon, Phys. Rev. Lett. **51**, 51 (1983).
[23] R. B. Laughlin, Phys. Rev. B **23**, 5632 (1981).
[24] J. L. Mañes, F. Guinea, and M. A. H. Vozmediano, Phys. Rev. B **75**, 155424 (2007).
[25] N. W. Ashcroft and N. D. Mermin, *Solid State Physics* (Cengage Learning, New York,1976).
[26] K. Sun, A. Souslov, X. Mao, and T. C. Lubensky, Proc. Natl. Acad. Sci. USA **109**, 12369 (2012).
[27] G. Wu, Y. Cho, I.-S. Choi, D. Ge, J. Li, H. N. Han, T. Lubensky, and S. Yang, Adv. Mater. **27**, 2747 (2015).
[28] J. Paulose, B. G.-g. Chen, and V. Vitelli, Nat. Phys. **11**, 153 (2015).